sustainability

MDPI

Article

Divergent Impacts of Climate Change and Human Activities on Vegetation Dynamics Across Land Use Types in Hunan Province, China

Qing Peng [1], Cheng Li [2,*], Xiaohong Fang [1], Zijie Wu [1], Kwok Pan Chun [3] and Thanti Octavianti [3]

[1] College of Geography and Tourism, Hengyang Normal University, Hengyang 421002, China
[2] Department of Ecology, School of Plant Protection, Yangzhou University, Yangzhou 225009, China
[3] CATE School of Architecture and Environment, University of the West of England, Bristol BS16 1QY, UK
* Correspondence: licheng@yzu.edu.cn

Abstract

Terrestrial ecosystems in Hunan Province have undergone marked yet spatially heterogeneous vegetation changes under concurrent climate change and intensifying human activities. The aim of this study is to resolve how vegetation responses vary among land-use types by quantifying kernel Normalized Difference Vegetation Index (kNDVI) dynamics during 2000–2023 using precipitation, temperature, and solar radiation, coupled with trend analysis and a partial-derivative-based attribution. Mean kNDVI increased overall at 0.0016 yr^{-1}; vegetation improved over 76.30% of the area, whereas 5.72% of the area experienced degradation. Built-up land exhibited the largest degraded fraction (35.04%). Human activities and temperature emerged as the dominant drivers of kNDVI change, contributing 62.25% and 27.92%, respectively, while precipitation (3.08%) and solar radiation (6.77%) played comparatively minor roles. Spatially, human activities primarily controlled vegetation dynamics in plains and urban clusters (~78% of the area), whereas temperature constrained vegetation in high-elevation mountain ranges. Analysis along the human footprint (HFP) gradient reveals that driver composition remains steady in resilient ecosystems (farmland and forest), despite increasing anthropogenic pressure, whereas fragile ecosystems (grassland and bareland) exhibited pronounced volatility and heightened sensitivity to environmental constraints. These findings provide a quantitative basis for developing sustainable ecological security strategies, incorporating region-specific measures such as adaptive afforestation, sustainable agricultural management, and strict ecological protection, to enhance ecosystem resilience by prioritizing the climate resilience of mountain forests and the stability of fragile grassland systems.

Keywords: vegetation dynamics; kNDVI; climate–human drivers; land-use types; partial-derivative attribution; HFP; Hunan

Check for updates

Academic Editor: Jan Hopmans

Received: 18 November 2025
Revised: 2 January 2026
Accepted: 5 January 2026
Published: 7 January 2026

Copyright: © 2026 by the authors. Licensee MDPI, Basel, Switzerland. This article is an open access article distributed under the terms and conditions of the Creative Commons Attribution (CC BY) license.

1. Introduction

Climate change and human activities are two primary drivers reshaping Earth's ecosystems [1]. Vegetation, as a core component of terrestrial ecosystems, regulates regional climate through its effects on surface albedo, roughness and evapotranspiration, conserves soil and water, and mediates the cycles of carbon, water and energy [2]. Changes in temperature, precipitation patterns, and incident solar radiation under climate change significantly affect vegetation phenology, species distributions, and ecosystem functions [3,4]. Warming can increase growing season length in many regions but also raises evaporative demand

and vapor pressure deficit, which intensifies soil moisture stress and heat damage [5]. Alterations in precipitation amount, seasonality and variability modify soil water availability, as well as the frequency of droughts and floods, thereby influencing vegetation growth, mortality and recovery following disturbances [6,7]. In addition, changes in cloud cover and aerosol loading alter the balance between direct and diffuse radiation, potentially enhancing or inhibiting canopy photosynthesis depending on the prevailing environmental conditions [8].

At the same time, human activities exert strong and spatially heterogeneous influences on vegetation. Land-use change, including farmland expansion, afforestation, deforestation and grassland conversion, directly alters species composition, canopy structure and rooting depth, and modifies surface albedo and roughness [9]. Urbanization increases impervious surface area and exacerbates urban heat-island effects, collectively reshaping local microclimates and contributing to vegetation water and heat stress [9,10]. Agricultural intensification, such as irrigation, fertilization and multiple cropping, can boost biomass and productivity but may reduce biodiversity and alter soil structure and biogeochemical cycling [11,12]. When these human pressures are superimposed on the climatic changes described above, their co-occurring influences on vegetation can be spatially heterogeneous and sometimes opposing [7,13,14]. For example, afforestation and ecological engineering can increase vegetation cover under favorable moisture conditions, but these gains may be difficult to sustain in regions where warming and drying reduce water availability [15]. Therefore, it is crucial to investigate long-term vegetation dynamics at the regional scale and to quantify the relative contributions of climate change and human activities, in order to support ecological security and sustainable development.

Vegetation dynamics, a key indicator of ecosystem health, can be effectively monitored using remote-sensing vegetation indices [4,16,17]. The traditional Normalized Difference Vegetation Index (NDVI) has been widely used to estimate vegetation growth due to its simplicity and accessibility [4,13]. However, NDVI is prone to saturation in densely vegetated areas and has limited sensitivity to changes in vegetation structure and function, which makes it difficult to capture subtle dynamics in complex ecosystems [18]. The recently proposed kernel Normalized Difference Vegetation Index (kNDVI) was designed to overcome these limitations through a non-linear spectral response that enhances sensitivity to physiological traits such as chlorophyll content and canopy structure [19]. kNDVI exhibits improved generalization, stability, and noise resistance, making it particularly suitable for monitoring vegetation in diverse and disturbed ecosystems [20]. Hence, kNDVI provides a more precise tool for assessing regional vegetation dynamics, especially in regions with dense canopies and pronounced human disturbance.

In recent years, a variety of approaches have been used to assess the relative impacts of climate change and human activities on vegetation dynamics, including statistical analysis methods, biophysical models, machine-learning techniques and partial derivatives methods [21–24]. Statistical methods often focus on the correlation strength rather than quantifying the magnitude of contribution [25]. Biophysical models, which simulate ecosystem or land-surface processes to estimate productivity and distinguish between human and climate influences, face challenges due to uncertain parameters and incomplete process representation, limiting their accuracy and applicability for regional-scale attribution [24]. Machine-learning approaches are frequently criticized as "black boxes" that prioritize prediction accuracy over the explicit decoupling of driving factors [24]. By contrast, the partial derivative-based attribution method offers a parsimonious and data-flexible framework [23,26–29]. It directly partitions observed vegetation trends into climatic and anthropogenic components, making it particularly well-suited for quantifying driver contributions under the heterogeneous conditions of Hunan Province.

Hunan Province, located in the middle and lower reaches of the Yangtze River, is a major agricultural and forestry region characterized by a typical subtropical monsoon climate [30]. The region is both a critical national food production area and an important ecological barrier. Over recent decades, Hunan has experienced rapid urbanization, infrastructure construction and resource development within the Yangtze River Economic Belt [22,31], while simultaneously being a key beneficiary of large-scale ecological restoration projects. This combination of humid monsoon climate, pronounced topographic gradients, and strong spatial contrasts in human disturbance creates an ideal setting to quantify spatial heterogeneity in vegetation trends and attribute the relative contributions of climate change and human activities. Previous studies in Hunan and the broader Yangtze River Basin have mainly focused on overall greening and large scale NDVI trends, or have examined the influence of single drivers at coarse spatial scales. However, while existing research has explored single drivers or macro-scale impacts, a quantitative attribution of how these drivers distinctively shape vegetation trends across different land use and land cover (LULC) types remains limited [16]. In particular, the specific contributions of key ecosystems such as forest, farmland and grassland to joint climatic and anthropogenic stresses, and the dominant drivers underlying these differences, have yet to be fully clarified. This knowledge gap constrains a deeper understanding of regional social ecological systems and limits the precision of ecological management and policy design.

Accordingly, the aim of this study is to assess the spatiotemporal patterns of vegetation dynamics and the relative contributions of climate change and human activities across different LULC types in Hunan Province, by integrating kNDVI with climatic variables and a partial-derivative-based attribution framework. Specifically, we aim: (1) to characterize the spatiotemporal trends of kNDVI-based vegetation dynamics over 2000–2023; (2) to quantify the relative contributions of precipitation, temperature, solar radiation and human activities to the observed kNDVI trends; and (3) to identify land-use-specific differences in trend characteristics and driver dominance by summarizing kNDVI trends and contribution terms across major LULC types. The findings are expected to inform region-specific ecological restoration and adaptive management practices in Hunan and the broader middle and lower Yangtze River region, and to provide insights for other regions that face similar dual pressures of climate change and socio-economic development.

2. Materials and Methods

2.1. Study Area

Hunan Province is located in the middle reaches of the Yangtze River (24°38′–30°08′ N, 108°47′–114°15′ E), covering about 2.12 × 10^5 km^2. The province exhibits a horseshoe-shaped basin topography, enclosed by mountains on the east, south, and west and descending toward the central and northern regions (Figure 1a). Major mountain ranges include the Wuling Mountains to the northwest, the Xuefeng Mountains to the west, the Nanling Mountains to the south, and the Luoxiao Mountains to the east, while the Dongting Lake Plain is situated in the north. Hunan has a subtropical humid monsoon climate with four distinct seasons and concurrent periods of precipitation and heat. The annual mean temperature ranges from 16 to 18 °C, and the average annual precipitation varies from 1200 to 1700 mm, decreasing from southeast to northwest [32]. These favorable hydrothermal conditions create an ideal environment for vegetation growth. Land cover in the region is dominated by forest, farmland, and built-up land (Figure 1b).

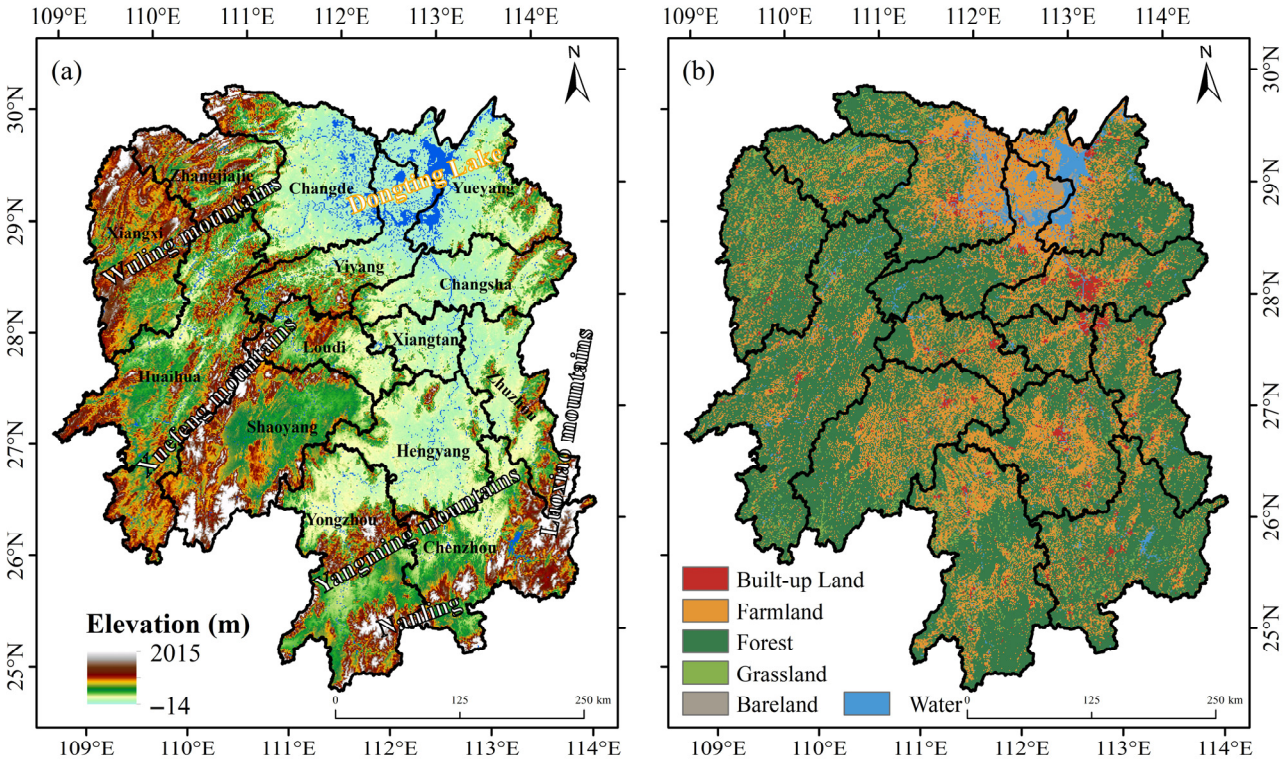


Figure 1. Topography (**a**) and land cover (**b**) 2020 of the study area.

In recent decades, Hunan has undergone marked climate warming and alterations in precipitation regimes, with more frequent hot extremes and heavy precipitation events [30,33]. These changes modify the thermal and moisture conditions for vegetation and affect growing-season length, vegetation productivity, and the occurrence of drought- and flood-related stress [5]. At the same time, Hunan is both a major grain-production base and a rapidly urbanizing province. Intensive rice-based agriculture dominates the Dongting Lake Plain and other low-lying basins, while surrounding mountains are covered by natural and planted forests that have been substantially modified by ecological restoration and ecological-engineering projects, generally enhancing vegetation cover on previously degraded slopes [34,35]. In contrast, the rapid expansion of the Changsha–Zhuzhou–Xiangtan urban agglomeration and other built-up areas, together with infrastructure construction and industrial and mining activities, has converted and fragmented cropland and forest, increasing local pressure on ecosystem services and vegetation conditions [31]. Overall, the superposition of climate change and diverse human activities produces pronounced spatial heterogeneity in vegetation dynamics across Hunan Province, providing a representative setting for assessing the coupled climatic and anthropogenic drivers of vegetation change.

2.2. Data Sources and Preprocessing

To ensure spatial consistency across the multi-source data and maintain analytical rigor, all raster data used in this study were resampled to a spatial resolution of 1 km. The data sources and preprocessing steps were as follows:

(1) Vegetation index data: The MOD13Q1 NDVI product, sourced from the National Aeronautics and Space Administration (NASA). This dataset has a spatial resolution of 250 m, a temporal resolution of 16 days, and spans the period from 2000 to 2023. Data processing was performed on the Google Earth Engine (GEE) platform [36,37], to enable efficient cloud-based preprocessing of long MODIS time series. The main steps included

outlier removal, clipping to the study area, resampling to 1 km using bilinear interpolation, and generating a monthly raster time series.

(2) Meteorological data: Monthly temperature and precipitation data with a 1 km resolution were obtained from the National Earth System Science Data Center (http://www.geodata.cn/, accessed on 20 May 2025), covering the period from 2000 to 2023. Solar radiation data were sourced from the TerraClimate global high-resolution monthly climate dataset [38]. These data were subsequently cropped and resampled on the GEE platform to a 1 km resolution to ensure spatial consistency with other datasets.

(3) Land use data: The 2020 LULC dataset, provided by the Resources and Environmental Science Data Center of the Chinese Academy of Sciences (https://www.resdc.cn/, accessed on 30 May 2025), was employed. This dataset features a resolution of 1 km. For the purpose of analysis, the original classifications were aggregated into six primary categories: forest, farmland, grassland, water, built-up land, and bareland. The 2020 LULC map was used as a static stratification to aggregate pixel-level kNDVI trends and contribution terms by land-use type.

(4) Human footprint data: The annual Human Footprint (HFP) dataset published by Mu et al. [39], with temporal coverage from 2000 to 2022 and a spatial resolution of 1 km, was used to quantify anthropogenic disturbance. This dataset integrates eight categories of human activity variables, including built environment, population density, night lights, cultivated land, pastures, railways, and navigable waterways, and can comprehensively reflect the intensity of regional human disturbance. In this study, the HFP data were used to characterize the intensity of anthropogenic pressure for the post hoc gradient analysis (Section 3.4) after the contribution decomposition.

2.3. Methods

This study aims to quantify spatiotemporal patterns and relative contributions of climate change and human activities to vegetation dynamics, represented by kNDVI, across different land use types in Hunan Province, China, during 2000–2023 (Figure 2). The analytical workflow includes four sequential components: (1) derivation of kNDVI from MODIS NDVI to mitigate saturation effects (Section 2.3.1); (2) spatiotemporal trend estimation and significance testing for kNDVI and climatic variables using non-parametric approaches (Section 2.3.2); (3) diagnostic analysis of climate–kNDVI associations using partial correlations to quantify independent relationships between kNDVI and each climatic driver (Section 2.3.3); and (4) a partial-derivative-based contribution decomposition to attribute the observed kNDVI trend to temperature, precipitation, solar radiation, and human activities (Section 2.3.4). In the attribution step, sensitivities of kNDVI to climatic drivers are estimated using a multiple linear regression model and combined with observed trend slopes within the partial-derivative-based decomposition.

2.3.1. kNDVI Calculation

To address the saturation limitation of the NDVI in densely vegetated areas, this study employed the kNDVI to assess vegetation dynamics [19]. It is calculated as follows:

$$kNDVI = \frac{k(NIR, red) - k(NIR, -red)}{k(NIR, red) + k(NIR, -red)} = \tanh\left[\left(\frac{NIR - red}{2\sigma}\right)^2\right] \quad (1)$$

where tanh denotes the hyperbolic tangent function, NIR and red represent the near-infrared and red bands, respectively, and σ controls sensitivity to sparse and dense vegetation. A commonly adopted value is σ = 0.5 (*NIR* + *red*), which leads to a simplified expression:

$$kNDVI = \tanh\left(NDVI^2\right) \quad (2)$$

where NDVI is the normalized difference vegetation index. Preliminary validation confirms that kNDVI effectively mitigates the saturation issue and exhibits a more normal distribution in our study area (see Figure S1 in Supplementary Material), making it a robust proxy for regional vegetation dynamics.

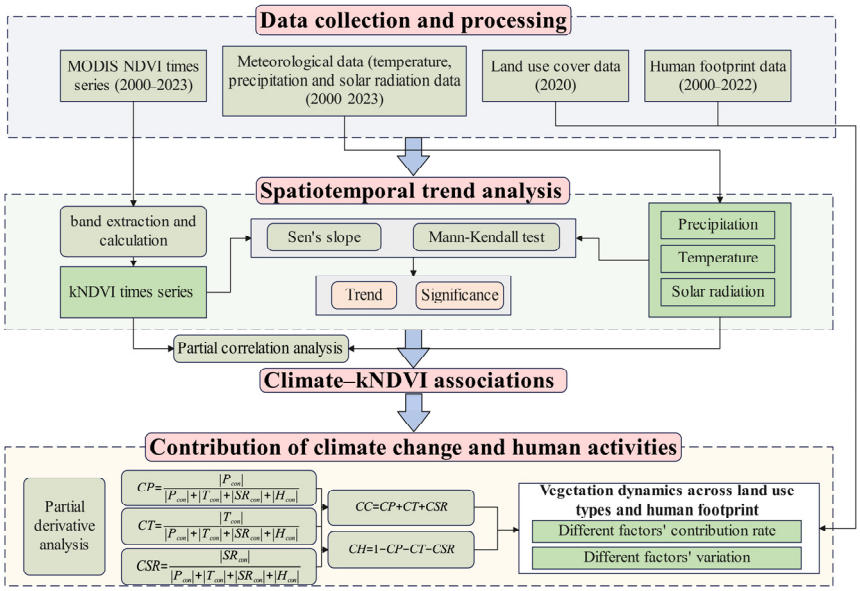


Figure 2. Technical flowchart of the study.

2.3.2. Trend Analysis and Significance Test

The Theil–Sen trend estimator and Mann–Kendall (MK) test are widely used non-parametric statistical methods for detecting monotonic trends in time series data [40]. The Theil–Sen estimator is used to calculate the slope of the trend, while the MK test is employed to assess its statistical significance. Together, these methods allow for the quantification of trend magnitude and significance, providing a comprehensive evaluation of long-term changes in kNDVI and associated climate variables. The Theil–Sen slope is calculated as:

$$slope = median\left(\frac{x_j - x_i}{j - i}\right), \forall j > i \quad (3)$$

where x_i and x_j are the values of kNDVI or meteorological variables at time steps i and j, respectively, with $i < j$. The resulting slope represents the median rate of change over the observation period.

The MK test uses the standardized statistic Z to assess the significance of the trend [13,25,40]. If $|Z| > 1.96$, the result is considered statistically significant at the 95% confidence level. Based on the results of both the Theil–Sen slope and MK test, trends in kNDVI and climate variables were classified into five categories of significance (Table 1).

Table 1. Significance types of trend changes in different indicators.

Slope	|Z|	Classification
>0.0005	>1.96	Significant improvement/increase
>0.0005	≤1.96	Slight improvement/increase
−0.0005~0.0005	≤1.96	Stability
<−0.0005	≤1.96	Slight degradation/decrease
<−0.0005	>1.96	Significant degradation/decrease

2.3.3. Partial Correlation Analysis

Partial correlation analysis was used to examine the relationship between two variables while controlling for the influence of other confounding variables [23,26,41]. Here, partial correlations were used as a complementary diagnostic to characterize independent climate–kNDVI association patterns, whereas the attribution of relative contributions was quantified using the partial-derivative-based decomposition described in Section 2.3.4. Specifically, this study employed partial correlation coefficients to quantify the independent responses of vegetation kNDVI to precipitation, mean temperature, and solar radiation. The Pearson correlation coefficient between variables x and y is defined as:

$$r_{xy} = \frac{\sum_{i=1}^{n}(x_i - \overline{x})(y_i - \overline{y})}{\sqrt{\sum_{i=1}^{n}(x_i - \overline{x})^2}\sqrt{\sum_{i=1}^{n}(y_i - \overline{y})^2}} \quad (4)$$

The first-order partial correlation coefficient, controlling for variable z, is calculated as:

$$r_{xy,z} = \frac{r_{xy} - r_{xz}r_{yz}}{\sqrt{(1 - r_{xz}{}^2)(1 - r_{yz}{}^2)}} \quad (5)$$

The second-order partial correlation coefficient, controlling for variables z and w, is given by:

$$r_{xy,zw} = \frac{r_{xy,z} - r_{xw,z}r_{yw,z}}{\sqrt{(1 - r_{xw,z}{}^2)(1 - r_{yw,z}{}^2)}} \quad (6)$$

where $\overline{x}$ and $\overline{y}$ are the mean values of the series of variables x and y, respectively; n is the length of the study time series; x_i and y_i are the values of x and y in year i, respectively; r_{xy}, r_{xz} and r_{zy} are the correlation coefficients between variables x and y, variables x and z, and variables y and z, respectively; $r_{xy,z}$ is the first-order partial correlation coefficient between variables x and y after excluding the influence of variable z; $r_{xy,zw}$ is the second-order partial correlation coefficient between x and y after excluding the influence of variables z and w; $r_{xy,z}$, $r_{xw,z}$ and $r_{yw,z}$ are the first-order partial correlation coefficients between variables x and y, x and w, and y and w, respectively.

2.3.4. Relative Contribution Decomposition Method

To quantify the relative contribution of climate change (C) and human activities (H) to vegetation dynamics, we employed the partial derivative-based decomposition method which has been widely applied for attribution of vegetation or ecohydrological changes in different regions and contexts [23,26–29]. This analytical framework assumes that the interannual variation in kNDVI represents the sum of contributions from climatic drivers (precipitation, temperature, and solar radiation) and a remaining non-climatic component, which is interpreted here primarily as human activities. The fundamental equation is expressed as:

$$\frac{d_{kNDVI}}{dt} \approx T_{con} + P_{con} + SR_{con} + H_{con} = \frac{\partial_{kNDVI}}{\partial T} \times \frac{dT}{dt} + \frac{\partial_{kNDVI}}{\partial P} \times \frac{dP}{dt} + \frac{\partial_{kNDVI}}{\partial SR} \times \frac{dSR}{dt} + H_{con} \quad (7)$$

where d_{kNDVI}/dt represents the interannual change rate of kNDVI, dT/dt, dP/dt, dSR/dt are the time derivatives (change rates) of temperature (T), precipitation (P), and solar radiation (SR), respectively. $\partial_{kNDVI}/\partial T$, $\partial_{kNDVI}/\partial P$ and $\partial_{kNDVI}/\partial SR$ denote the regression coefficients of T, P and SR, respectively, estimated from a multiple linear regression model that includes T, P and SR simultaneously. To assess potential multicollinearity among climatic drivers, we calculated the Variance Inflation Factor (VIF). VIF values for all predictors were consistently below 5 (Figure S2 in the Supplementary Material), suggesting that multicollinearity is unlikely to materially bias the estimated coefficients. T_{con}, P_{con},

SR_{con} and H_{con} represent the contributions of T, P, SR, and H to the variations in kNDVI, respectively. The H_{con} was derived as follows:

$$H_{con} = \frac{d_{kNDVI}}{dt} - \frac{\partial_{kNDVI}}{\partial T} \times \frac{dT}{dt} - \frac{\partial_{kNDVI}}{\partial P} \times \frac{dP}{dt} - \frac{\partial_{kNDVI}}{\partial SR} \times \frac{dSR}{dt} \quad (8)$$

Based on these components, the relative contributions are calculated as:

$$CT = \frac{|T_{con}|}{|T_{con}| + |P_{con}| + |SR_{con}| + |H_{con}|} \quad (9)$$

$$CP = \frac{|P_{con}|}{|T_{con}| + |P_{con}| + |SR_{con}| + |H_{con}|} \quad (10)$$

$$CSR = \frac{|SR_{con}|}{|T_{con}| + |P_{con}| + |SR_{con}| + |H_{con}|} \quad (11)$$

$$CC = CT + CP + CSR \quad (12)$$

$$CH = 1 - CC \quad (13)$$

where CC, CT, CP, CSR and CH are used to represent the relative contribution rates T, P, SR, C and H to the changes in kNDVI, respectively.

3. Results

3.1. Spatiotemporal Characteristics of Vegetation kNDVI

Vegetation kNDVI across Hunan Province is generally high but exhibits strong spatial heterogeneity that reflects a persistent high-mountain versus low-basin contrast. Higher values occur in the mountainous and hilly regions of western, southern, and eastern Hunan, whereas lower values are concentrated in the horseshoe-shaped central basin and the northern Dongting Lake Plain (Figure 3a). Although interannual variability is evident during 2000–2023, the spatial pattern remained largely stable. Over the same period, the provincial mean kNDVI increased significantly by 0.0016 yr^{-1} ($p < 0.05$; Figure 3b), indicating an overall greening signal at the provincial scale.

At the pixel level, greening dominated across most of the province, whereas browning was clustered in lowland plains and major urbanized areas. Specifically, kNDVI increased across 76.30% of the land area, with 51.86% exhibiting statistically significant greening (Figure 4a,b). Declines occurred over 13.60% of the province, including 5.72% with significant browning, and these areas were mainly concentrated in the Dongting Lake Plain and several major urbanized cities, whereas the remaining 10.10% showed non-significant trend. Municipal level statistics are consistent with these regional contrasts. Changsha was the only municipality that showed a decrease in kNDVI over 2000–2023, with a mean slope of -0.0001 yr^{-1}, whereas all other municipalities exhibited positive trends. Xiangxi Autonomous Prefecture exhibited the strongest greening trend with a mean slope of 0.0027 yr^{-1}. Changde and Yiyang showed comparatively weak greening relative to the provincial average, with mean slopes of 0.0006 yr^{-1} and 0.0008 yr^{-1}, respectively.

Land use stratification further highlights systematic differences in trend magnitude and the prevalence of degradation hotspots (Figure 4c,d). Forest, grassland, and farmland increased significantly at 0.0020 yr^{-1}, 0.0024 yr^{-1}, and 0.0009 yr^{-1}, respectively, bareland increased non-significantly at 0.0007 yr^{-1}, whereas built-up land decreased significantly at -0.0022 yr^{-1}. Despite the overall greening signal, improvement and degradation coexisted within each land use type. Degradation was most pronounced in built-up land, where significant and slight declines accounted for 35.04% and 17.07% of that category, respectively. Localized decreases were also present in farmland, forest, grassland, and

bareland, with decreasing kNDVI accounting for 23.91% of farmland area, 13.50% of forest area, 10.89% of grassland area, and 26.44% of bareland area. Overall, provincial scale greening is the dominant feature, while browning hotspots persist particularly in built-up areas and parts of the lowland plains, which indicates persistent degradation hotspots within human-dominated landscapes.

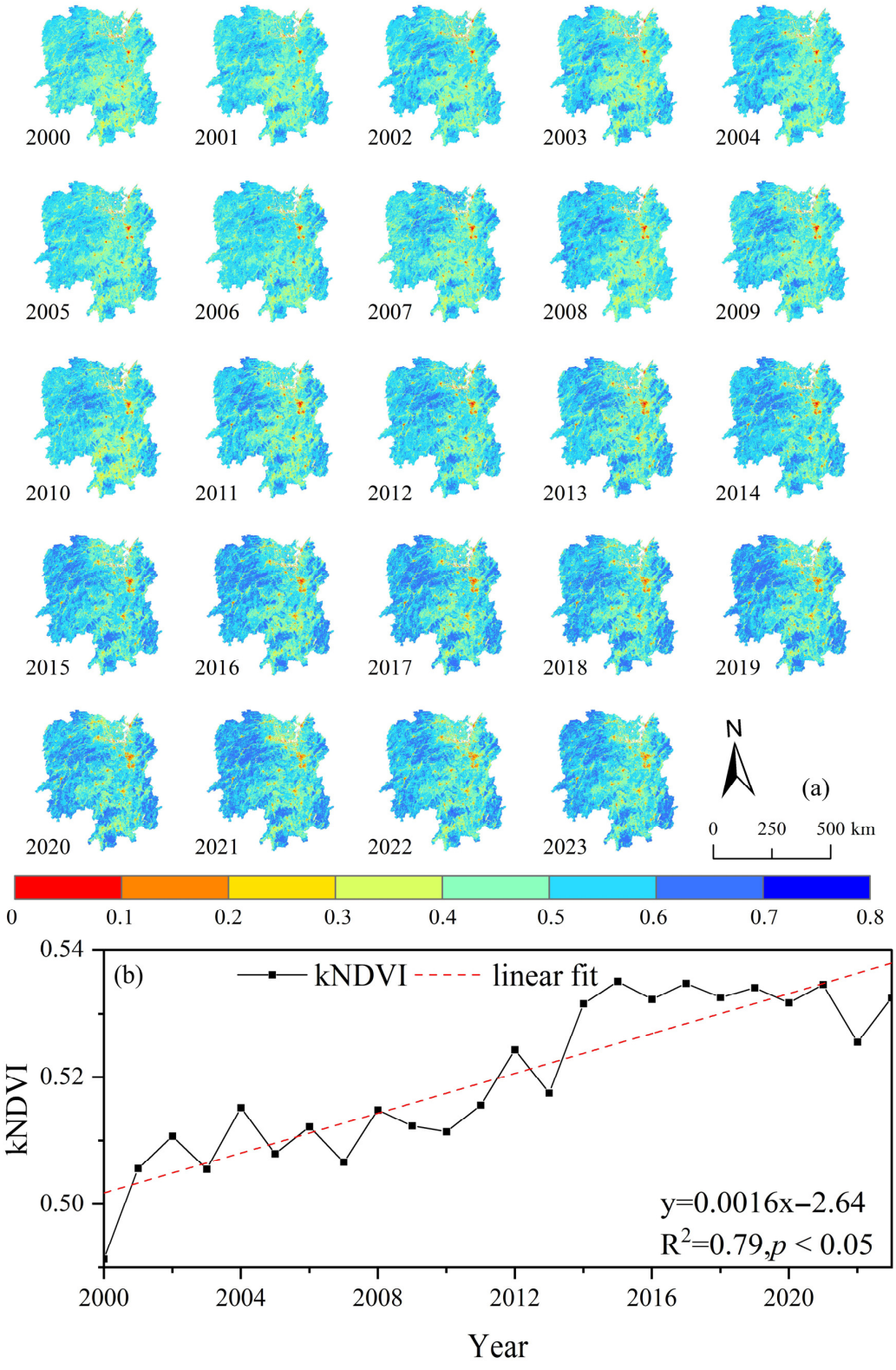


Figure 3. Spatial distribution map of kNDVI in Hunan from 2000 to 2023 (**a**) and annual change trend map (**b**).

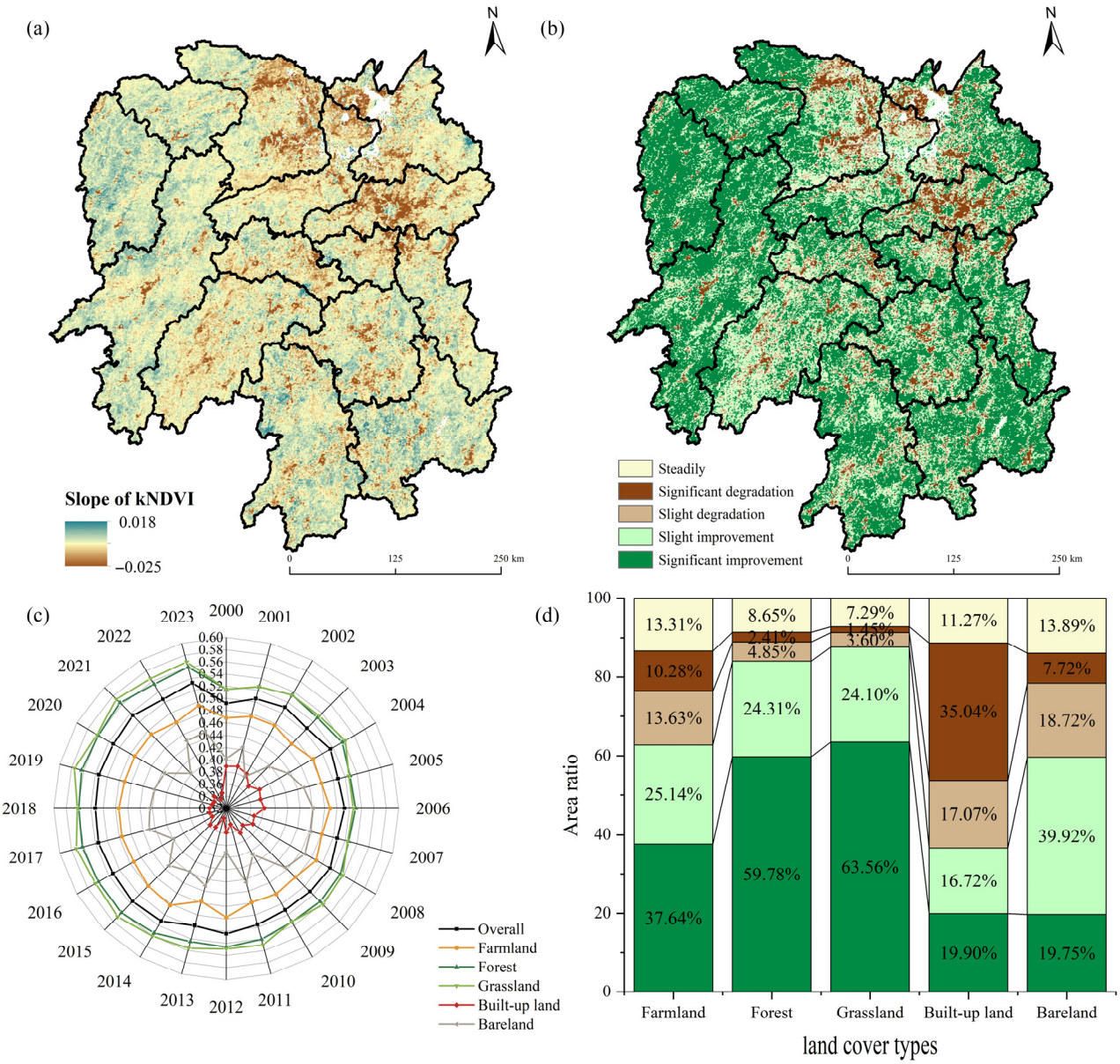


Figure 4. kNDVI spatial trend change and statistical analysis. (**a**) kNDVI spatial trend change. (**b**) kNDVI trend type. (**c**) Annual change in mean kNDVI for different land use types. (**d**) Area proportion of different kNDVI trend types for different land use types.

3.2. Characteristics of Climate Factor Variations and Their Impacts on Vegetation Dynamics

Across 2000 to 2023, precipitation and temperature increased across land use types, while solar radiation declined, and the climate–kNDVI associations differed systematically among land use categories (Figure 5). Precipitation exhibited an overall increasing trend across the province, characterized by marked interannual variability and distinct spatial heterogeneity. Historically, forest and grassland ecosystems received the highest annual precipitation volumes, whereas bareland areas remained comparatively drier (Figure 5a). Over the study period, precipitation increased across all land use types (Figure 5b), with the steepest rises observed in grassland (2.53 mm yr^{-1}) and forest (1.72 mm yr^{-1}). Partial correlation patterns indicate that precipitation was positively associated with kNDVI in built-up land and farmland, whereas the relationship is negative in grassland and bareland. Built-up land and farmland showed positive partial correlations that exceed the regional mean (red dashed line), indicating a stronger linkage between precipitation variability and kNDVI in these land use types. In contrast, grassland and bareland exhibited negative

correlations, indicating an inverse precipitation–kNDVI association in these landscapes when temperature and solar radiation are held constant.

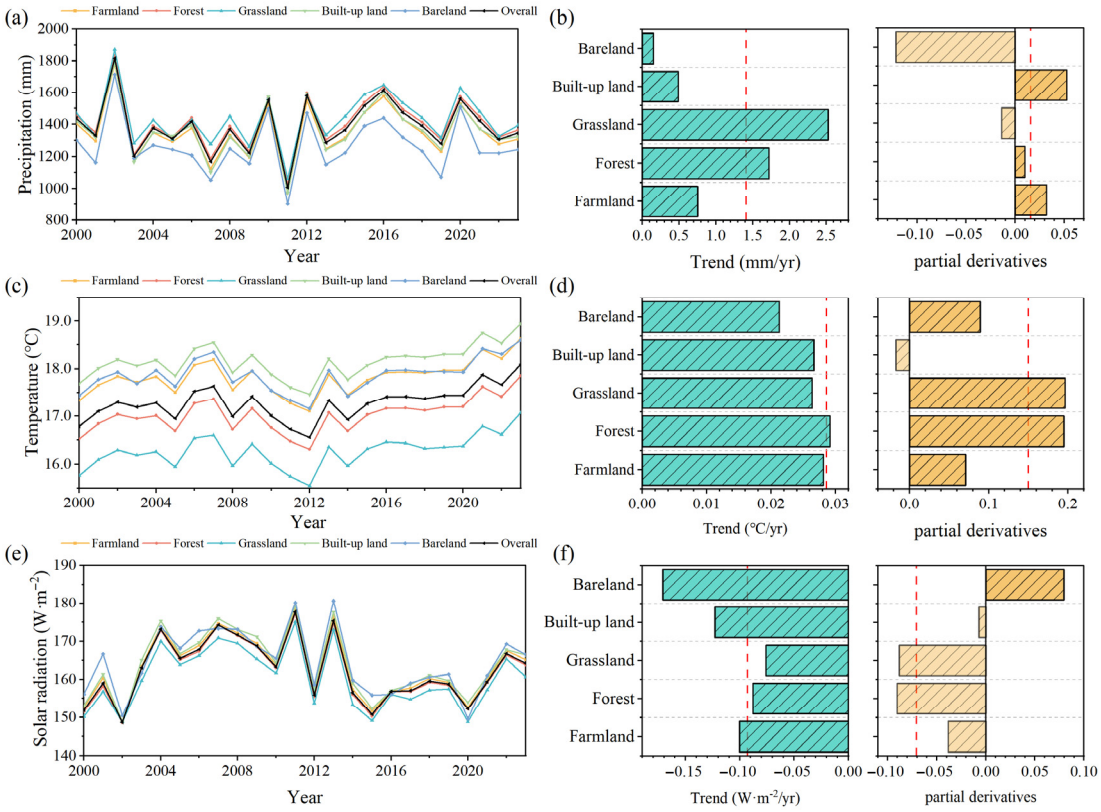


Figure 5. Annual mean changes in meteorological factors (precipitation, temperature, solar radiation) for different land use types (**a**,**c**,**e**), trend changes in each factor and their partial correlation coefficients with kNDVI (**b**,**d**,**f**). The red dotted lines indicate the regional mean (area-averaged) values.

Temperature showed the clearest land use stratification and was positively associated with kNDVI in most land use types, with the strongest associations in forest and grassland. Spatially, a clear thermal stratification was evident (Figure 5c), with built-up land and bareland generally exhibiting higher mean temperatures than the cooler, vegetation-dense forest and grassland areas. Temporally, temperatures increased across all land use types (Figure 5d), with the highest warming rate in forest (0.029 °C yr^{-1}), followed by farmland (0.028 °C yr^{-1}) and built-up land (0.027 °C yr^{-1}). In terms of impact, partial correlation analysis revealed a predominantly positive associations to warming, whereas bareland exhibited a distinct negative correlation. Forest and grassland showed relatively high positive associations, with coefficients of 0.20 and 0.19, indicating a stronger association between temperature variability and vegetation greenness in these ecosystems.

Solar radiation declined across all land use types with relatively synchronized interannual fluctuations, and its associations with kNDVI were predominantly negative except over bareland. Annual mean solar radiation exhibits a different pattern from precipitation and temperature (Figure 5e). Values are similar among land use types, with no pronounced stratification, and interannual fluctuations are highly synchronized. Solar radiation decreased across all land use types (Figure 5f). The decreases are most pronounced over bareland and built-up land, at 0.17 W m^{-2} yr^{-1} and 0.12 W m^{-2} yr^{-1}, respectively, both more pronounced than the regional mean (red dashed line). Forest and grassland show more gradual declines, with rates smaller than the regional mean. Partial correlations indicate a positive correlation between solar radiation and kNDVI only over bareland, whereas farmland, forest, grassland, and built-up land show negative correlations. The

strongest negative partial correlations were observed in forest and grassland. This pattern indicates the strongest inverse solar radiation–kNDVI association among land use types when precipitation and temperature are held constant.

3.3. Quantification of Contribution Rate

Using a partial-derivative method, we quantitatively decomposed the relative contributions of climatic factors (precipitation, temperature, and solar radiation) and human activities to kNDVI variations across different land use types in the study area. Overall, the spatial attribution highlights two dominant patterns. Human activities explain the majority of kNDVI change across most lowland plains and urban clusters, whereas temperature is the leading climatic contributor and is most prominent in mountainous regions (Figure 6).

Among climatic drivers, temperature accounted for the largest share of kNDVI change. The contribution rate of temperature (CT) averaged 27.92% across the province. High CT values were mainly concentrated in high-elevation areas such as the Wuling Mountains, Xuefeng Mountains, and Nanling Mountains (Figure 6b). At the municipal scale, Chenzhou, situated in the Nanling range, records the highest mean CT of 42.66%, followed by Zhuzhou at 35.43%, indicating a larger temperature contribution in these high-elevation areas (Table 2). In contrast, precipitation and solar radiation played subordinate roles. The contribution rate of precipitation (CP) was low throughout the region, with a regional mean of only 3.08% (Figure 6a). Even in western municipalities such as Huaihua and Xiangxi, the mean contributions remained low at 4.27% and 4.12%, respectively (Table 2). Similarly, the contribution rate of solar radiation (CSR) averaged 6.77% and showed no distinct large-scale clusters of high values (Figure 6c). CSR was relatively higher in northern plains municipalities such as Changde, which averaged 13.54%, compared to western areas (Table 2). The combined climate contribution (CC) had a regional mean of 37.78% (Figure 6d) and its spatial pattern closely resembled that of CT.

Table 2. Mean contribution rates of driving factors at the municipal scale.

Municipality	Mean Contribution Rate (%)			
	CP	CT	CSR	CH
Changde	3.26	21.38	13.54	61.83
Yueyang	2.77	24.79	10.79	61.66
Zhangjiajie	1.21	25.19	8.46	65.14
Yiyang	3.06	18.32	10.32	68.3
Xiangxi	4.12	24.7	5.24	65.94
Huaihua	4.27	29.67	3.71	62.35
Changsha	2.27	20.78	8.88	68.06
Loudi	2.85	19.94	5.6	71.61
Xiangtan	1.47	21.34	7.15	70.05
Zhuzhou	1.31	35.43	4.32	58.94
Shaoyang	3.76	30.11	3.64	62.5
Hengyang	1.41	29.61	4.2	64.77
Chenzhou	3.25	42.66	7.34	46.75
Yongzhou	3.91	29.78	5.89	60.42

CP: contribution rate of precipitation, CT: contribution rate of temperature, CSR: contribution rate of solar radiation, CH: contribution rate of human activities.

Human activities exert an overwhelmingly dominant influence across the study area, surpassing the combined influence of all climatic factors. The contribution rate of human activities (CH) averaged 62.25% (Figure 6e). High-contribution zones extensively cover the Dongting Lake Plain and other low-lying basins in the central lowlands, particularly around the Changsha-Zhuzhou-Xiangtan urban agglomeration and adjacent built-up ar-

eas, indicating that non-climatic factors currently exert dominant control on vegetation dynamics in this region. This dominance peaks in the municipalities of Loudi (71.61%), Xiangtan (70.05%), and Changsha (68.06%). This spatial contrast indicates that non-climatic influences dominate in lowland human-dominated landscapes, whereas climatic influences become relatively more apparent in high-elevation ecological barriers.

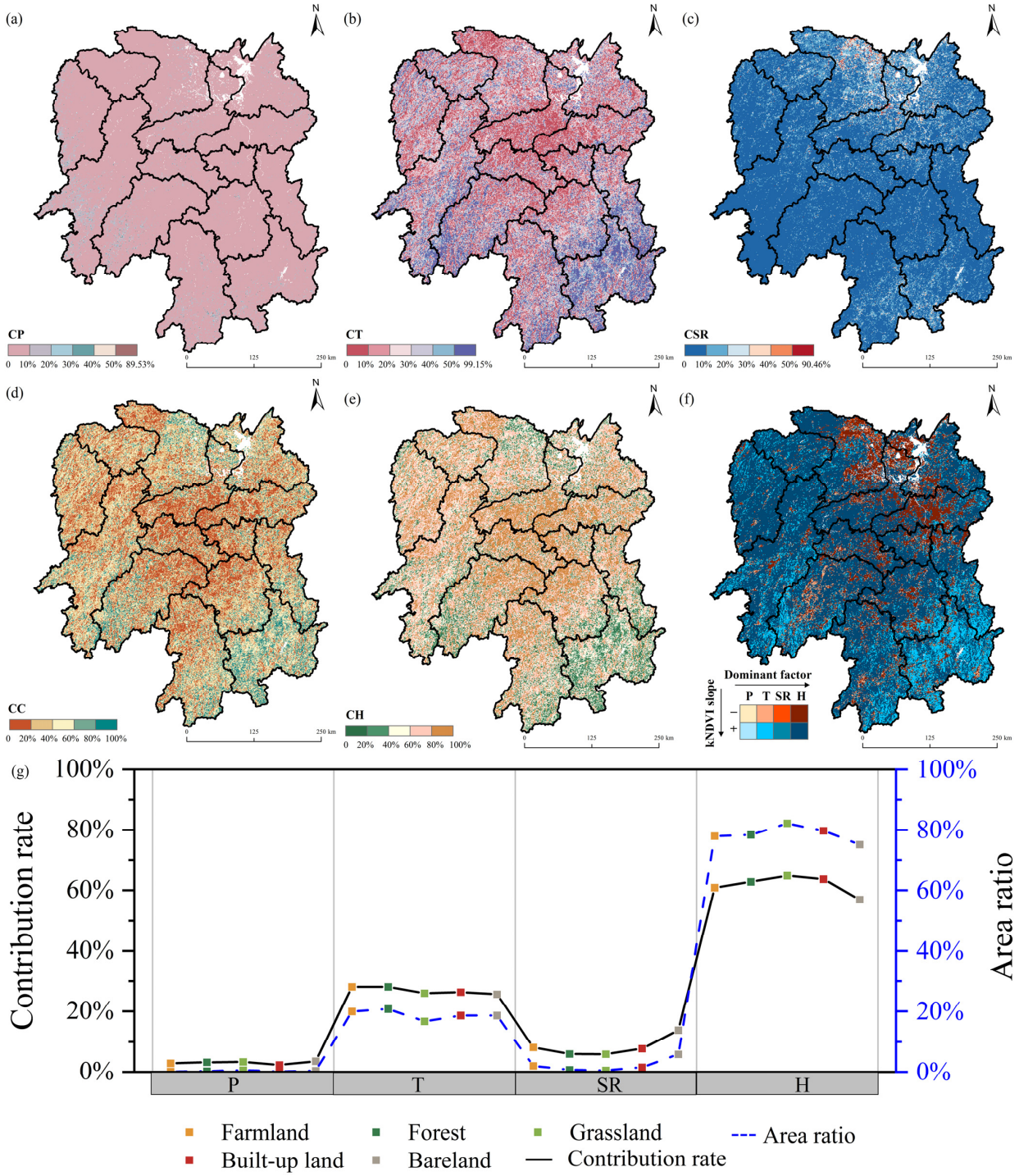


Figure 6. Contributions of different influencing factors to kNDVI variation. (**a**) Precipitation contribution (CP). (**b**) Temperature contribution (CT). (**c**) Solar radiation contribution (CSR). (**d**) Climate contribution (CC). (**e**) Contribution from human activities (CH). (**f**) Dominant factors influencing kNDVI at the gridscale. (**g**) Contributions of various factors to kNDVI variation under different land use types and the proportion of land area covered by dominant factors. Values are expressed as percentages.

The spatial dominance of human-related contributions differed between greening and browning pixels (Figure 6f). Areas classified as human-activity dominated accounted for ~78.38% of the province. In areas with increasing kNDVI, the human-related component was predominantly positive and explained 79.88% of the total contribution magnitude. In contrast, in pixels with decreasing kNDVI, the human-related component remains dominant (71.52%) but was predominantly negative. Climatic influences also show regime-dependent behavior. Temperature accounts for 19.35% of the contribution magnitude in greening areas, mainly across high-elevation ecological barriers, but increases to 24.44% in browning areas. Similarly, the relative contribution of solar radiation rises from 0.63% in greening zones to 3.58% in browning zones. Together, these patterns suggest that human-related factors largely shape the overall spatial pattern, while browning pixels show a larger relative share of climatic contributions than greening pixels.

Across land use types, anthropogenic dominance was pervasive, indicating that even natural ecosystems are strongly shaped by management interventions (Figure 6g). Within areas dominated by human activity, the mean contribution of human activities consistently exceeds 60%, indicating strong control across all major land types. With respect to the proportion of dominant area, grassland and built-up land exhibit the highest shares governed by human activity (82.17% and 79.72%, respectively), followed closely by forest and farmland (78.35% and 77.95%). These patterns indicate that human activities exert a pervasive influence on regional vegetation. Human interventions not only strongly influence artificial ecosystems such as built-up land and farmland but also affect natural or semi-natural ecosystems, including grassland and forest, through ecological restoration projects, forestry management, and other disturbances. As a result, these ecosystems are primarily governed by non-climatic factors. In temperature-dominated zones, forest has the largest proportion of area primarily controlled by temperature (20.73%), slightly higher than farmland (19.93%) and built-up land (18.60%), and markedly higher than grassland (16.72%). This suggests that, compared with other land use types, forest ecosystems, particularly those at higher elevations, are more sensitive to thermal conditions and retain a stronger imprint of natural climatic variability, especially temperature limitations.

3.4. Effects of Human Activities on Vegetation Change

The spatial distribution of anthropogenic pressure showed a clear core to periphery pattern that is consistent with the regional urbanization and land management intensity. High HFP values were concentrated in central urban cores and adjacent intensively managed agricultural areas (Figure 7a). Municipal statistics support this spatial clustering, with Changsha and Xiangtan exhibiting the highest mean HFP values of 18.06 and 17.87, respectively. In contrast, lower HFP values were more common in mountainous peripheral regions, where Zhangjiajie and Huaihua recorded the lowest mean HFP values of 11.74 and 11.76, respectively.

HFP intensity differed substantially among land use types, consistent with a gradient from highly managed to less disturbed landscapes (Figure 7b). Mean HFP followed the order of built-up land, farmland, forest, grassland, and bareland. Built-up land had the highest mean HFP of 29.08, reflecting concentrated human infrastructure and activity. Farmland ranks second with a mean HFP of 17.34, consistent with intensive land management. Bareland had the lowest mean HFP, indicating relatively limited direct human footprint in these areas within the HFP framework.

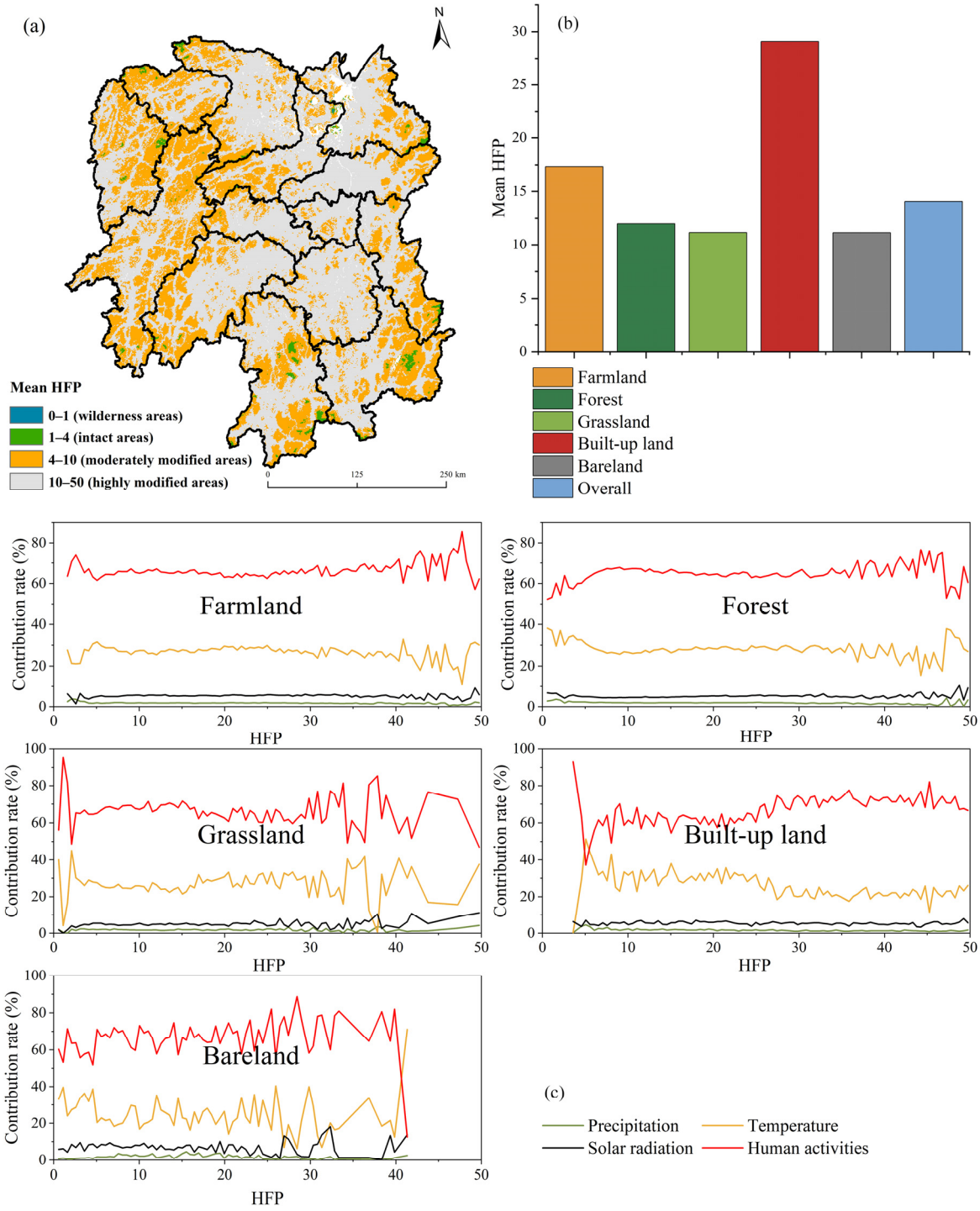


Figure 7. Spatial distribution of the Human Footprint (HFP) and factor contributions to vegetation change. (**a**) Mean HFP from 2000 to 2022. (**b**) Mean HFP across land use types. (**c**) CP, CT, CSR, and CH to kNDVI change along the HFP gradient across land use types.

The contribution patterns along the HFP gradient varied by land use type, with relatively stable attribution in major land systems and higher variability in marginal land use types (Figure 7c). In farmland, forest, and built-up land, the relative contributions changed only modestly across most of the HFP range. Human activities generally accounted for about 60% to 75%, with temperature providing a steady secondary influence of about 25% to 30%. This indicates that for these land types, anthropogenic effects remain the dominant component across a wide range of disturbance intensity. In contrast, grassland

and bareland exhibited larger variability along the HFP gradient. Grassland showed wider swings in the human activity contribution, ranging from about 50% to 80%, suggesting a less stable driver structure. Bareland exhibited the highest variability with irregular shifts among drivers, indicating that attribution patterns in these marginal lands are more sensitive to local conditions and disturbances. Overall, the gradient analysis suggests that anthropogenic dominance is a persistent feature for the major land use types, whereas marginal ecosystems show more volatile attribution patterns along the HFP gradient.

4. Discussion

4.1. Vegetation Greening Trends and Ecological Restoration

From 2000 to 2023, vegetation in Hunan Province exhibited a significant and widespread greening trend, consistent with the broad-scale ecological recovery observed in the Yangtze River Basin [3,9,42]. A robust feature is that greening aligns spatially with restoration priority areas and land management patterns, which is consistent with a leading role of policy-driven interventions, with climate variability acting as an enabling background condition rather than a sole driver.

This interpretation is supported by two lines of evidence. First, greening is strongest in mountainous and hilly regions where major national restoration programs were preferentially implemented, including the Grain for Green Program, the Yangtze River Shelterbelt System, and the Natural Forest Conservation Program [15,43]. Second, the attribution consistently assigns the largest share of kNDVI change to the human-related component, indicating that non-climatic influences dominate the long-term trend signal in many areas. Together, these findings are consistent with previous assessments that ecological engineering and land management have contributed substantially to greening in China, especially in regions targeted for erosion control and ecological security [3,15,17].

However, this restoration success is spatially counterbalanced by urbanization-induced constraints. Urbanizing lowland areas show weaker greening and localized browning, consistent with land conversion to impervious surfaces and degradation pressures associated with rapid development [10,44]. Furthermore, attributing greening solely to human intervention would overlook the essential co-regulation by climate. While ecological engineering expanded vegetation cover, relatively favorable climatic conditions provided the water availability necessary for vegetation establishment and persistence [15,43]. This dependence implies vulnerability, since a shift toward drier conditions or more frequent hot drought extremes could limit the maintenance of restored vegetation [45,46]. In addition, as large-scale ecological projects mature, marginal gains in greenness may approach saturation, while urbanization and climate extremes may increasingly govern year to year fluctuations and degradation risks [5,47,48]. Consequently, future efforts should shift from pursuing coverage expansion alone to enhancing ecosystem quality and resilience.

4.2. Impact of Driving Factors on Vegetation Dynamics

A central outcome of the attribution is that temperature is the leading climatic contributor to kNDVI change in Hunan, while precipitation and solar radiation contribute smaller shares in the long-term trend decomposition. This pattern is consistent with the energy-limited view that in humid regions vegetation is often more strongly regulated by energy-related factors than by annual water supply [14,46]. Under Hunan's generally abundant precipitation, interannual rainfall variability may be less limiting at the annual scale, which is consistent with the modest precipitation contribution estimated by the decomposition.

However, interannual variability indicates that hydrological extremes can still exert a disproportionate influence on year-to-year vegetation anomalies. As observed in our

results (Section 3.2), years with extreme precipitation peaks (e.g., 2002, 2012) coincided with distinct vegetation growth anomalies. In the subtropical monsoon climate, seasonal droughts frequently occur during hot summers [42]. Therefore, extreme rainfall years may have played a compensatory role by mitigating seasonal water deficits, boosting annual kNDVI. This phenomenon aligns with the "positive asymmetry" hypothesis, where carbon gains in wet years often exceed losses in dry years [49]. Conversely, compound extremes, such as the 2013 heatwave-drought event, can override thermal benefits, causing significant browning [50]. Taken together, these contrasts suggest that resilience depends not only on mean climate trends but also on the timing and intensity of hydrological extremes.

The dominant role of human activities further emphasizes that vegetation dynamics are deeply reshaped by management. The spatial match between high HFP and vegetation greening in agricultural zones suggests that intensive management practices (e.g., fertilization, irrigation) may mitigate the dependence of crop growth on natural climate constraints [9,12,30].

4.3. Differentiated Responses Across Land Use Types

Land use stratification clarifies how the balance of climate and human influence differs among ecosystem types, which helps connect the spatial patterns to plausible drivers. In Built-up land, human interference acts as a primary stressor. The significant decline in kNDVI and its negative correlation with temperature (Figures 4c and 5d) are consistent with heat-related constraints. The Urban Heat Island (UHI) effect can exacerbate local warming, increasing evaporative demand and intensifying water stress [10,31,44]. Extreme heat in these impervious landscapes often exceeds species-specific thermal optima, suppressing photosynthesis [31,51,52].

In farmland, the dominance of the human-related component and the comparatively weaker climate associations are consistent with intensive management that stabilizes productivity under climate variability, including irrigation and fertilization practices [9,11,12]. This interpretation aligns with prior work indicating that management can partially decouple crop greenness from background climate constraints.

Forest and grassland retain stronger climate sensitivity than farmland and built-up land, which is consistent with their exposure to natural climatic variability and the absence of uniform management buffering. The positive associations with temperature are consistent with warming alleviating thermal constraints in montane environments and extending the growing season [53]. At the same time, the negative solar radiation associations in forest and grassland should be interpreted as statistical relationships conditional on precipitation and temperature, rather than as direct evidence of a specific radiation mechanism. One plausible explanation is that higher irradiance co-occurs with hotter and drier conditions that elevate evaporative demand and constrain greenness, which would generate an inverse association in a humid subtropical setting. Another plausible explanation is a role for diffuse radiation effects under aerosol driven dimming, which has been discussed in the literature [8,54–56]. These hypotheses cannot be distinguished with annual statistics alone, and distinguishing them would require seasonal analysis and explicit information on cloud and aerosol variability.

In contrast to forests, grassland kNDVI correlates negatively with precipitation. This divergence is likely governed by root-depth dependent hydrological regulation [57]. Grasslands in Hunan typically possess shallower root systems compared to woody forests. During the intensive monsoon season, excessive precipitation can induce temporary surface soil saturation and soil hypoxia [58]. Literature suggests that such waterlogging can inhibit root respiration and nutrient uptake, creating a physiological stress that likely contributes to suppressing vegetation growth despite the abundance of water. Forests, with

deeper rooting profiles and higher transpiration capacity, are better equipped to buffer these hydrological extremes, whereas shallow-rooted grasslands exhibit heightened sensitivity to "wet" stress [57,58].

4.4. Policy Implication and Adaptive Management Strategies

These results suggest that future ecological restoration should shift from simply expanding vegetation cover to enhancing ecosystem quality and resilience, consistent with recent national calls for high-quality, function-oriented restoration [1,15]. In ecological barrier regions such as mountainous areas in Chenzhou, vegetation is strongly constrained by temperature. Our results, together with previous work on forest productivity and climate sensitivity in subtropical China, indicate that warming can both relax low-temperature limitations and increase exposure to heat and drought stress in montane forests [34,53]. Policies should therefore focus on enhancing forest thermal resilience, for example, by prioritizing heat- and stress-tolerant tree species, maintaining structurally diverse stands, and critically, matching afforestation strategies with local edaphic conditions. Specifically, in the karst landscape areas of western and southern Hunan characterized by thin soil layers and low water retention, restoration strategies should prioritize drought-tolerant shrubs or grass-shrub mosaics over high-density forests. This adaptive approach prevents excessive transpiration-induced soil drying, thereby mitigating the risk of ecological degradation under warming climates [24,45].

In urban agglomerations, the priority is to minimize the negative impacts of urban expansion and to mitigate the urban heat island, which imposes combined thermal and water stress on urban vegetation [10,31]. Integrating green infrastructure into planning, expanding urban green spaces and adopting drought- and heat-tolerant species can help cool the urban environment and improve vegetation condition [51].

Transitional zones dominated by grassland and bareland exhibit the largest variability along the human footprint gradient and are therefore particularly fragile. The negative correlation between grassland kNDVI and precipitation suggests a risk of waterlogging stress during the monsoon season, which is consistent with experimental and synthesis studies showing that shallow-rooted systems are highly sensitive to soil saturation, hypoxia and associated reductions in nutrient uptake [57,58]. In these areas, management should control land-use intensity, improve soil drainage and promote waterlogging-tolerant grass species to enhance resilience to extreme hydrological events.

By contrast, farmland ecosystems, although strongly controlled by human activities, show relatively high stability. The strong dominance of human contributions, together with evidence that precision irrigation and improved fertilizer management can increase yields, water-use efficiency and soil organic carbon, highlights the importance of sustainable agricultural practices. Promoting such practices is essential for maintaining stable production while safeguarding water and soil resources [12,35].

4.5. Limitations and Future Research Directions

Although this study integrates multi-source datasets and applies a quantitative decomposition framework to investigate the drivers of vegetation dynamics, several methodological and data-related constraints merit consideration. A primary limitation lies in the attribution framework, which relies on a linear additive response model to quantify climatic effects. Specifically, the sensitivities of kNDVI to precipitation, temperature, and solar radiation are estimated as coefficients from a multiple linear regression model in which these climatic predictors act simultaneously. While this approach allows a transparent first-order partitioning of dkNDVI/dt, it remains a simplification that may underrepresent nonlinear responses and interactive effects among climatic stressors. For example, the co-occurrence

of heatwaves and drought can amplify vegetation stress beyond what would be expected from the sum of individual effects [20,46]. VIF values remained low throughout the study period (Figure S2), indicating limited multicollinearity and suggesting that collinearity is unlikely to materially bias the estimated coefficients. Nevertheless, the linear model does not explicitly capture threshold behavior, lagged responses, or higher-order interactions; future work could employ generalized additive models or machine-learning–based attribution to better characterize these nonlinear synergies. We therefore interpret the attribution as a first-order, spatially explicit partitioning of the observed kNDVI trend among covarying drivers, rather than as process-level causality.

Spatiotemporal uncertainties also arise from the stratification strategy. The reliance on a static 2020 LULC map involves a necessary trade-off between regional consistency and dynamic precision. While this establishes a stable baseline for comparing ecosystem types, it inherently smooths over land conversion processes in transition zones. To evaluate uncertainty introduced by this stratification, we performed a post hoc sensitivity analysis using the land-use transition matrix from 2000 to 2020 (Figure S3 and Table S1). The results indicate that the landscape structure in Hunan is macroscopically stable. Forest and farmland, which cover >90% of the province, exhibited marginal net area changes of −0.33% and −0.98%, respectively, supporting the use of the 2020 LULC map as a robust baseline for these dominant ecosystems.

Crucially, for pixels undergoing significant transitions, the non-climatic residual term (H_{con}) dominated the trend signal. In areas converted from farmland to built-up land, H_{con} accounted for 64.28% of the total trend, substantially exceeding the summed climatic contribution; similarly, for forest-to-built-up transitions, the residual contribution remained high at 63.57%. These results are consistent with strong anthropogenic influences associated with land-use conversion, while we note that H_{con} is a residual term that may also include other non-climatic processes (e.g., CO_2 fertilization [17,59], nitrogen deposition, management practices) and data uncertainties. Utilizing annual land-cover products and incorporating additional human-related covariates would offer finer granularity in distinguishing the impacts of land-use change from land-use management and reduce residual ambiguity.

In addition, the analysis focuses on concurrent annual relationships, which may not fully resolve time-lagged ecological responses or fine-scale heterogeneity. Vegetation growth often exhibits memory effects, where physiological damage from extreme climatic events suppresses productivity in subsequent years [60]. Such lagged responses and unmeasured biogeochemical drivers are partly absorbed by the residual component and model error. To address these complexities, future work should prioritize integrating nonlinear modeling frameworks, such as distributed lag models or deep learning, to explicitly quantify time-lagged effects. Furthermore, combining broad-scale satellite observations with high-resolution data and ground-based monitoring will be essential to validate these mechanisms across diverse micro-environments.

5. Conclusions

This study systematically analyzed vegetation dynamics in Hunan Province from 2000 to 2023 and their responses to climate and human activities. The main conclusions are as follows.

(1) Hunan Province has experienced significant vegetation greening over the past two decades. Higher vegetation levels and more persistent improvements occurred in mountainous regions, while lower vegetation levels were concentrated in the central basin and the Dongting Lake Plain.

(2) The dominant controls on vegetation change differ systematically across landscapes. In high-elevation ecological barriers, vegetation responses are more closely linked to

temperature conditions, consistent with an energy-limited environment in which warming can alleviate thermal constraints. In contrast, in low lying basins and human-dominated zones, including the Dongting Lake Plain and the Changsha-Zhuzhou-Xiangtan urban agglomeration and other built-up areas, anthropogenic influences play a stronger role and are associated with weaker greening signals.

(3) These spatially differentiated controls imply that ecosystem management should be tailored to landscape context rather than applied uniformly. Mountain forests may require resilience-oriented conservation under continued warming, whereas intensively managed agricultural basins and urbanizing areas would benefit from planning led adaptive management, including strategies that limit the negative impacts of expansion and strengthen urban green infrastructure.

(4) Overall, climate constrains the biophysical potential for vegetation growth, whereas human activities increasingly shape the realized trajectory of regional ecosystems. Quantitative attribution here should be interpreted as first order evidence because the partial-derivative based method relies on linear and static relationships and does not explicitly represent nonlinear interactions or lagged responses.

Supplementary Materials: The following supporting information can be downloaded at: https://www.mdpi.com/article/10.3390/su18020621/s1, Figure S1: Empirical comparison between multi-year mean (2000–2023) NDVI and kNDVI in Hunan Province (excluding water bodies). (a) Scatter plot illustrating NDVI compression at high values and the wider dynamic range of kNDVI. (b) Histograms comparing the distributions of NDVI and kNDVI; Figure S2: Interannual variation in VIF for climatic drivers (precipitation, temperature, and solar radiation) during 2000–2023; Figure S3: Sankey diagram illustrating land use transitions in Hunan Province from 2000 to 2020; Table S1: Mean contribution rates of climatic factors and human activities to vegetation dynamics across different land use transition types (2000–2020).

Author Contributions: Conceptualization, methodology, Q.P. and C.L.; software, formal analysis, writing—original draft, Q.P. and X.F.; writing—review & editing, Z.W., K.P.C. and T.O.; funding acquisition, Q.P. and X.F. All authors have read and agreed to the published version of the manuscript.

Funding: This research was funded by the Scientific Research Funds of Hunan Provincial Education Department (Grant No. 23B0677), Department of Science and Technology of Hunan province (Grant No. 2022JJ40014), the Research Initiation Project of Hengyang Normal University (Grant Nos. 2022QD10, 2022QD13, 2022QD09), the Research Program of Humanities and Social Sciences of the Ministry of Education (Grant No. 25YJCZH117).

Institutional Review Board Statement: Not applicable.

Informed Consent Statement: Not applicable.

Data Availability Statement: The original contributions presented in this study are included in the article/Supplementary Materials. Further inquiries can be directed to the corresponding author.

Acknowledgments: We are grateful to all the platforms that supplied data. Moreover, we sincerely thank the editors and anonymous reviewers for their valuable input and advice on this manuscript.

Conflicts of Interest: The authors declare that they have no known competing financial interests or personal relationships that could have appeared to influence the work reported in this paper.

References

1. Calvin, K.; Dasgupta, D.; Krinner, G.; Mukherji, A.; Thorne, P.W.; Trisos, C.; Romero, J.; Aldunce, P.; Barrett, K.; Blanco, G. *IPCC, 2023: Climate Change 2023: Synthesis Report. Contribution of Working Groups I, II and III to the Sixth Assessment Report of the Intergovernmental Panel on Climate Change; Core Writing Team*; Lee, H., Romero, J., Eds.; IPCC: Geneva, Switzerland, 2023.
2. Gerten, D.; Schaphoff, S.; Haberlandt, U.; Lucht, W.; Sitch, S. Terrestrial Vegetation and Water Balance—Hydrological Evaluation of a Dynamic Global Vegetation Model. *J. Hydrol.* **2004**, *286*, 249–270. [CrossRef]

3. Piao, S.; Yin, G.; Tan, J.; Cheng, L.; Huang, M.; Li, Y.; Liu, R.; Mao, J.; Myneni, R.B.; Peng, S. Detection and Attribution of Vegetation Greening Trend in China over the Last 30 Years. *Glob. Change Biol.* **2015**, *21*, 1601–1609. [CrossRef] [PubMed]
4. Ozyavuz, M.; Bilgili, B.; Salıcı, A. Determination of Vegetation Changes with NDVI Method. *J. Environ. Prot. Ecol.* **2015**, *16*, 264–273.
5. Yan, Y.; Liu, Z.; Chen, L.; Chen, X.; Lin, K.; Zeng, Z.; Lan, X.; Huang, L.; Wang, Y.; Yao, L. Earth Greening and Climate Change Reshaping the Patterns of Terrestrial Water Sinks and Sources. *Proc. Natl. Acad. Sci. USA* **2025**, *122*, e2410881122. [CrossRef]
6. Allen, C.D.; Macalady, A.K.; Chenchouni, H.; Bachelet, D.; McDowell, N.; Vennetier, M.; Kitzberger, T.; Rigling, A.; Breshears, D.D.; Hogg, E.H.; et al. A Global Overview of Drought and Heat-Induced Tree Mortality Reveals Emerging Climate Change Risks for Forests. *For. Ecol. Manag.* **2010**, *259*, 660–684. [CrossRef]
7. Liu, N.; Ding, Y.; Peng, S. Temporal effects of climate on vegetation trigger the response biases of vegetation to human activities. *Glob. Ecol. Conserv.* **2021**, *31*, e01822. [CrossRef]
8. Kanniah, K.D.; Beringer, J.; North, P.; Hutley, L. Control of Atmospheric Particles on Diffuse Radiation and Terrestrial Plant Productivity: A Review. *Prog. Phys. Geogr.* **2012**, *36*, 209–237. [CrossRef]
9. Chen, C.; Park, T.; Wang, X.; Piao, S.; Xu, B.; Chaturvedi, R.K.; Fuchs, R.; Brovkin, V.; Ciais, P.; Fensholt, R. China and India Lead in Greening of the World through Land-Use Management. *Nat. Sustain.* **2019**, *2*, 122–129. [CrossRef]
10. Seto, K.C.; Güneralp, B.; Hutyra, L.R. Global Forecasts of Urban Expansion to 2030 and Direct Impacts on Biodiversity and Carbon Pools. *Proc. Natl. Acad. Sci. USA* **2012**, *109*, 16083–16088. [CrossRef]
11. Ren, K.; Wang, Z.; Wu, J.; Zhao, K.; Huang, M.; Li, Y. One− off Irrigation Enhances Wheat Yield and Water Productivity: Evidence from Meta− Analysis and a Three− Year and Three− Site Field Experiment. *Agric. Water Manag.* **2025**, *317*, 109628. [CrossRef]
12. Tao, J.; Liu, X. Combined Application of Nitrogen and Phosphorus Fertilizers Increases Soil Organic Carbon Storage in Cropland Soils. *Eur. J. Agron.* **2025**, *168*, 127607. [CrossRef]
13. Jin, H.; Chen, X.; Wang, Y.; Zhong, R.; Zhao, T.; Liu, Z.; Tu, X. Spatio-Temporal Distribution of NDVI and Its Influencing Factors in China. *J. Hydrol.* **2021**, *603*, 127129. [CrossRef]
14. Nemani, R.R.; Keeling, C.D.; Hashimoto, H.; Jolly, W.M.; Piper, S.C.; Tucker, C.J.; Myneni, R.B.; Running, S.W. Climate-Driven Increases in Global Terrestrial Net Primary Production from 1982 to 1999. *Science* **2003**, *300*, 1560–1563. [CrossRef]
15. Song, W.; Feng, Y.; Wang, Z. Ecological Restoration Programs Dominate Vegetation Greening in China. *Sci. Total Environ.* **2022**, *848*, 157729. [CrossRef] [PubMed]
16. Yuan, J.; Xu, Y.; Xiang, J.; Wu, L.; Wang, D. Spatiotemporal Variation of Vegetation Coverage and Its Associated Influence Factor Analysis in the Yangtze River Delta, Eastern China. *Environ. Sci. Pollut. Res.* **2019**, *26*, 32866–32879. [CrossRef]
17. Zhu, Z.; Piao, S.; Myneni, R.B.; Huang, M.; Zeng, Z.; Canadell, J.G.; Ciais, P.; Sitch, S.; Friedlingstein, P.; Arneth, A. Greening of the Earth and Its Drivers. *Nat. Clim. Chang.* **2016**, *6*, 791–795. [CrossRef]
18. Zhu, C.; Tian, J.; Tian, Q.; Wang, X.; Li, Q. Using NDVI-NSSI Feature Space for Simultaneous Estimation of Fractional Cover of Non-Photosynthetic Vegetation and Photosynthetic Vegetation. *Int. J. Appl. Earth Obs. Geoinf.* **2023**, *118*, 103282. [CrossRef]
19. Camps-Valls, G.; Campos-Taberner, M.; Moreno-Martínez, Á.; Walther, S.; Duveiller, G.; Cescatti, A.; Mahecha, M.D.; Muñoz-Marí, J.; García-Haro, F.J.; Guanter, L. A Unified Vegetation Index for Quantifying the Terrestrial Biosphere. *Sci. Adv.* **2021**, *7*, eabc7447. [CrossRef]
20. Wang, J.; Bao, Z.; Wang, G.; Liu, C.; Xie, M.; Wang, B.; Zhang, J. The Time Lag Effects and Interaction among Climate, Soil Moisture, and Vegetation from In Situ Monitoring Measurements across China. *Remote. Sens.* **2024**, *16*, 2063. [CrossRef]
21. Piao, S.; Wang, X.; Park, T.; Chen, C.; Lian, X.; He, Y.; Bjerke, J.W.; Chen, A.; Ciais, P.; Tømmervik, H.; et al. Characteristics, Drivers and Feedbacks of Global Greening. *Nat. Rev. Earth Environ.* **2020**, *1*, 14–27. [CrossRef]
22. Qu, S.; Wang, L.; Lin, A.; Zhu, H.; Yuan, M. What Drives the Vegetation Restoration in Yangtze River Basin, China: Climate Change or Anthropogenic Factors? *Ecol. Indic.* **2018**, *90*, 438–450. [CrossRef]
23. Peng, Q.; Wang, R.; Jiang, Y.; Li, C. Contributions of Climate Change and Human Activities to Vegetation Dynamics in Qilian Mountain National Park, Northwest China. *Glob. Ecol. Conserv.* **2021**, *32*, e01947. [CrossRef]
24. Shi, Y.; Jin, N.; Ma, X.; Wu, B.; He, Q.; Yue, C.; Yu, Q. Attribution of Climate and Human Activities to Vegetation Change in China Using Machine Learning Techniques. *Agric. For. Meteorol.* **2020**, *294*, 108146. [CrossRef]
25. Tuoku, L.; Wu, Z.; Men, B. Impacts of Climate Factors and Human Activities on NDVI Change in China. *Ecol. Inform.* **2024**, *81*, 102555. [CrossRef]
26. Ma, B.; Wang, S.; Mupenzi, C.; Li, H.; Ma, J.; Li, Z. Quantitative Contributions of Climate Change and Human Activities to Vegetation Changes in the Upper White Nile River. *Remote Sens.* **2021**, *13*, 3648. [CrossRef]
27. Ge, W.; Deng, L.; Wang, F.; Han, J. Quantifying the Contributions of Human Activities and Climate Change to Vegetation Net Primary Productivity Dynamics in China from 2001 to 2016. *Sci. Total Environ.* **2021**, *773*, 145648. [CrossRef]
28. Shrestha, B.; Zhang, L.; Shrestha, S.; Khadka, N.; Maharjan, L. Spatiotemporal Patterns, Sustainability, and Primary Drivers of NDVI-Derived Vegetation Dynamics (2003–2022) in Nepal. *Environ. Monit. Assess.* **2024**, *196*, 607. [CrossRef]

29. Naeem, S.; Zhang, Y.; Li, C.; Li, Y.; Azeem, T.; Mahmood, R. Estimation and Attribution of Nonlinear Trend of Water Use Efficiency Using a Normalized Partial Derivative Approach. *J. Environ. Manag.* **2024**, *372*, 123323. [CrossRef]
30. Hui, J.; Cheng, Y. Evolution and Spatiotemporal Response of Ecological Environment Quality to Human Activities and Climate: Case Study of Hunan Province, China. *Remote Sens.* **2024**, *16*, 2380. [CrossRef]
31. Li, J.; Wang, J.; Zhou, W. Different Impacts of Urbanization on Ecosystem Services Supply and Demand across Old, New and Non-Urban Areas in the ChangZhuTan Urban Agglomeration, China. *Landsc. Ecol.* **2024**, *39*, 107. [CrossRef]
32. Chen, L.-C.; Wang, S.-L.; Wang, Q.-K. Ecosystem Carbon Stocks in a Forest Chronosequence in Hunan Province, South China. *Plant Soil* **2016**, *409*, 217–228. [CrossRef]
33. Chen, A.; He, X.; Guan, H.; Cai, Y. Trends and Periodicity of Daily Temperature and Precipitation Extremes during 1960–2013 in Hunan Province, Central South China. *Theor. Appl. Climatol.* **2018**, *132*, 71–88. [CrossRef]
34. Zhang, Q.; Xiao, J.; Meng, X.; Ma, J.; He, P. Spatial Heterogeneity Analysis of the Driving Mechanisms and Threshold Responses of Vegetation at Different Regional Scales in Hunan Province. *Forests* **2025**, *16*, 515. [CrossRef]
35. Xiang, H.; Zhou, C.; Cuidong; Song, H. High-Quality Agricultural Development in the Central China: Empirical Analysis Based on the Dongting Lake Area. *Geomatica* **2024**, *76*, 100010. [CrossRef]
36. Valerio, F.; Godinho, S.; Marques, A.T.; Crispim-Mendes, T.; Pita, R.; Silva, J.P. GEE_xtract: High-Quality Remote Sensing Data Preparation and Extraction for Multiple Spatio-Temporal Ecological Scaling. *Ecol. Inform.* **2024**, *80*, 102502. [CrossRef]
37. Amani, M.; Ghorbanian, A.; Ahmadi, S.A.; Kakooei, M.; Moghimi, A.; Mirmazloumi, S.M.; Moghaddam, S.H.A.; Mahdavi, S.; Ghahremanloo, M.; Parsian, S.; et al. Google Earth Engine Cloud Computing Platform for Remote Sensing Big Data Applications: A Comprehensive Review. *IEEE J. Sel. Top. Appl. Earth Obs. Remote Sens.* **2020**, *13*, 5326–5350. [CrossRef]
38. Abatzoglou, J.T.; Dobrowski, S.Z.; Parks, S.A.; Hegewisch, K.C. TerraClimate, a High-Resolution Global Dataset of Monthly Climate and Climatic Water Balance from 1958–2015. *Sci. Data* **2018**, *5*, 1–12. [CrossRef]
39. Mu, H.; Li, X.; Wen, Y.; Huang, J.; Du, P.; Su, W.; Miao, S.; Geng, M. A Global Record of Annual Terrestrial Human Footprint Dataset from 2000 to 2018. *Sci. Data* **2022**, *9*, 176. [CrossRef]
40. Gocic, M.; Trajkovic, S. Analysis of Changes in Meteorological Variables Using Mann-Kendall and Sen's Slope Estimator Statistical Tests in Serbia. *Glob. Planet. Change* **2013**, *100*, 172–182. [CrossRef]
41. Jiang, M.; Tian, S.; Zheng, Z.; Zhan, Q.; He, Y. Human Activity Influences on Vegetation Cover Changes in Beijing, China, from 2000 to 2015. *Remote Sens.* **2017**, *9*, 271. [CrossRef]
42. Qu, S.; Wang, L.; Lin, A.; Yu, D.; Yuan, M.; Li, C. Distinguishing the Impacts of Climate Change and Anthropogenic Factors on Vegetation Dynamics in the Yangtze River Basin, China. *Ecol. Indic.* **2020**, *108*, 105724. [CrossRef]
43. Dou, Y.; Tong, X.; Horion, S.; Feng, L.; Fensholt, R.; Shao, Q.; Tian, F. The Success of Ecological Engineering Projects on Vegetation Restoration in China Strongly Depends on Climatic Conditions. *Sci. Total Environ.* **2024**, *915*, 170041. [CrossRef] [PubMed]
44. van Vliet, J. Direct and Indirect Loss of Natural Area from Urban Expansion. *Nat. Sustain.* **2019**, *2*, 755–763. [CrossRef]
45. Simonson, W.D.; Miller, E.; Jones, A.; García-Rangel, S.; Thornton, H.; McOwen, C. Enhancing Climate Change Resilience of Ecological Restoration—A Framework for Action. *Perspect. Ecol. Conserv.* **2021**, *19*, 300–310. [CrossRef]
46. Zhao, Y.; Jiang, Q.; Wang, Z. Nonlinear Spatiotemporal Variability of Gross Primary Production in China's Terrestrial Ecosystems under Water Energy Constraints. *Environ. Res.* **2025**, *269*, 120919. [CrossRef]
47. Thibault, K.M.; Brown, J.H. Impact of an Extreme Climatic Event on Community Assembly. *Proc. Natl. Acad. Sci. USA* **2008**, *105*, 3410–3415. [CrossRef]
48. Du, J.; Fu, Q.; Fang, S.; Wu, J.; He, P.; Quan, Z. Effects of Rapid Urbanization on Vegetation Cover in the Metropolises of China over the Last Four Decades. *Ecol. Indic.* **2019**, *107*, 105458. [CrossRef]
49. Dai, L.; Yang, Y.; Wang, X.; Yang, G.; Liang, M.; Hu, Z. Positive Asymmetric Responses Indicate Larger Carbon Sink with Increase in Precipitation Variability in Global Terrestrial Ecosystems. *Innov. Geosci.* **2024**, *2*, 100060. [CrossRef]
50. Yuan, W.; Cai, W.; Chen, Y.; Liu, S.; Dong, W.; Zhang, H.; Yu, G.; Chen, Z.; He, H.; Guo, W.; et al. Severe Summer Heatwave and Drought Strongly Reduced Carbon Uptake in Southern China. *Sci. Rep.* **2016**, *6*, 18813. [CrossRef]
51. Pataki, D.E.; Carreiro, M.M.; Cherrier, J.; Grulke, N.E.; Jennings, V.; Pincetl, S.; Pouyat, R.V.; Whitlow, T.H.; Zipperer, W.C. Coupling Biogeochemical Cycles in Urban Environments: Ecosystem Services, Green Solutions, and Misconceptions. *Front. Ecol. Environ.* **2011**, *9*, 27–36. [CrossRef]
52. Zhao, L.; Lee, X.; Smith, R.B.; Oleson, K. Strong Contributions of Local Background Climate to Urban Heat Islands. *Nature* **2014**, *511*, 216–219. [CrossRef] [PubMed]
53. Ji, Y.; Zhou, G.; Luo, T.; Dan, Y.; Zhou, L.; Lv, X. Variation of Net Primary Productivity and Its Drivers in China's Forests during 2000–2018. *Forest Ecosystems* **2020**, *7*, 15. [CrossRef]
54. Durand, M.; Murchie, E.H.; Lindfors, A.V.; Urban, O.; Aphalo, P.J.; Robson, T.M. Diffuse Solar Radiation and Canopy Photosynthesis in a Changing Environment. *Agric. For. Meteorol.* **2021**, *311*, 108684. [CrossRef]
55. Wild, M. Global Dimming and Brightening: A Review. *J. Geophys. Res. Atmos.* **2009**, *114*, D00D16. [CrossRef]

56. Mercado, L.M.; Bellouin, N.; Sitch, S.; Boucher, O.; Huntingford, C.; Wild, M.; Cox, P.M. Impact of Changes in Diffuse Radiation on the Global Land Carbon Sink. *Nature* **2009**, *458*, 1014–1017. [CrossRef]
57. Fan, Y.; Miguez-Macho, G.; Jobbágy, E.G.; Jackson, R.B.; Otero-Casal, C. Hydrologic Regulation of Plant Rooting Depth. *Proc. Natl. Acad. Sci. USA* **2017**, *114*, 10572–10577. [CrossRef]
58. Pan, N.; Feng, X.; Fu, B.; Wang, S.; Ji, F.; Pan, S. Increasing Global Vegetation Browning Hidden in Overall Vegetation Greening: Insights from Time-Varying Trends. *Remote Sens. Environ.* **2018**, *214*, 59–72. [CrossRef]
59. Donohue, R.J.; Roderick, M.L.; McVicar, T.R.; Farquhar, G.D. Impact of CO_2 Fertilization on Maximum Foliage Cover across the Globe's Warm, Arid Environments. *Geophys. Res. Lett.* **2013**, *40*, 3031–3035. [CrossRef]
60. Wu, D.; Zhao, X.; Liang, S.; Zhou, T.; Huang, K.; Tang, B.; Zhao, W. Time-Lag Effects of Global Vegetation Responses to Climate Change. *Glob. Change Biol.* **2015**, *21*, 3520–3531. [CrossRef]

Disclaimer/Publisher's Note: The statements, opinions and data contained in all publications are solely those of the individual author(s) and contributor(s) and not of MDPI and/or the editor(s). MDPI and/or the editor(s) disclaim responsibility for any injury to people or property resulting from any ideas, methods, instructions or products referred to in the content.